ELSEVIER

Nuclear Instruments and Methods in Physics Research A 444 (2000) 546–556

NUCLEAR INSTRUMENTS & METHODS IN PHYSICS RESEARCH Section A

www.elsevier.nl/locate/nima

Optics design and performance of LESB3, a two-stage separated 800-MeV/c kaon beamline

J. Doornbos[a,*], P. Pile[b], F. Meot[c], M. Aoki[a,1], E.W. Blackmore[a], I-H. Chang[b], C.J. Kost[a], K.K. Li[b], J.A. Macdonald[a], T. Nakano[a,2]

[a] *TRIUMF, Vancouver, B.C., V6T 2A3, Canada*
[b] *Brookhaven National Laboratory, Upton, NY 11973, USA*
[c] *DSM/DAPNIA/SEA, CEA Saclay, F-91191 Gif-sur-Yvette, Cedex, France*

Received 29 September 1999; accepted 22 October 1999

Abstract

The optics design and the measured performance are described for LESB3, the 800-MeV/c kaon beamline at the Brookhaven AGS used by E787 to search for rare K^+ decays. The beamline provides a flux of $\sim 5\times10^5 K^+/10^{12}$ protons on target, with a K/π ratio of > 3. © 2000 Elsevier Science B.V. All rights reserved.

Keywords: Brookhaven AGS; Secondary beam; Kaon beam; Separated beam; Wien filter; Beam optics

1. Introduction

Charged kaon beams are accompanied by other particles such as pions and protons from the production target which are typically a few hundred to a thousand times more abundant than the kaons. For momenta below a few GeV/c, usually a Wien separator (velocity filter) is used which transmits kaons while giving a vertical angle kick to other particles in the beam. The succeeding optics transforms this kick to a displacement in vertical position at a vertical focus, where these particles are intercepted by a mass slit. By this technique, the measured contamination in one-stage separated kaon beams is substantially reduced, but still higher than the kaon intensity, by a factor of 2–5 for K^+ and a factor of 6–15 for K^-.

Much of this remaining contamination can be eliminated in a two-stage separated beam. The technique of two-stage separated beams has been used succesfully in long beamlines with a small-angle acceptance [1]. The first separator and mass slit reduce the contamination by about one order of magnitude and create a well-defined source for the second stage. However, as experiments required higher kaon rates, shorter one-stage separated beams with larger angle acceptance were built, and the high total particle rates from the increased contamination could be dealt with up to a point by improvements in detector design. The objective of

* Corresponding author. Tel.: +1-604-222-1047; fax: +1-604-222-1074.
E-mail address: trjd@triumf.ca (J. Doornbos).
[1] Present address: National Laboratory for High Energy Physics (KEK), 1-1 Oho, Tsukuba, Ibaraki, 305 Japan.
[2] Present address: Department of Physics, Osaka University, 1-1 Machikaneyama, Toyonaka, Osaka, 560 Japan.

0168-9002/00/$ - see front matter © 2000 Elsevier Science B.V. All rights reserved.
PII: S0168-9002(99)01178-X

Experiment 787 at the Brookhaven National Laboratory Alternating Gradient Synchrotron (BNL AGS) is to measure the branching ratio of the rare decay $K^+ \to \pi + \nu\bar{\nu}$ which is predicted by second-order effects in the Standard Model at the level of 10^{-10}. The initial phase of this experiment achieved a sensitivity about an order of magnitude above this level [2] running at a momentum of 800 MeV/c on the Low Energy Separated Beam 1 (LESB1) with a small solid angle acceptance and π/K flux ratio ~ 2.5. Further gains in sensitivity from increased intensity of the primary 24-GeV proton beam were limited by losses from deadtime and accidental backgrounds due in part to contamination in the K^+ beam.

In order to reach the needed sensitivity, the detector was upgraded to improve resolution and rate capability, and the channel was upgraded to provide a pure K^+ beam with increased flux. The new two-stage separated beam LESB3 has a factor of 2.5 gain in kaon intensity and a factor of 10 smaller π contamination than LESB1. The new channel has a factor 4 higher solid angle acceptance which more than compensates for decay losses in the additional length needed for the second separator stage. The beam runs routinely with a kaon rate that is 3 times higher than the mostly pion contamination. At the time of the design of the beam, a 1.8-GeV/c two-stage separated K^- beamline was being constructed at BNL [3]. It employed sextupoles and octupoles to correct second- and third-order optics aberations. An innovative set of four independently movable jaws before the first separation stage was used to further reject contamination that still passes through the two mass slits. These features have been incorporated into the present beamline design. This paper describes the issues involved in the optics design of this high-flux pure kaon beam. The intensity of the proton beam was of the order of 10^{13} protons per pulse. The technical aspects of the beam design, including the design of the production target and the radiation hard front end will be described in a separate report.

In Section 2 the reasons for the contamination are discussed. Sections 3 and 4 give the layout and the design of the beam optics. Section 5 describes the results of Monte Carlo calculations. In Section 6 a comparison is made between measurements and design expectations. Section 7 summarizes conclusions.

2. Sources of contamination in kaon beams

The contamination can originate from several potential sources. In the case of LESB3 higher-order aberrations are large because of the large-angle acceptance. Since the first quadrupole is placed very close to the 6-cm long production target there is a severe "depth of focus" effect. The optics differ over the length of the target, making it difficult to correct the higher-order aberrations which cause a long tail on the vertical pion profiles at the mass slits, and a small fraction of the pions directly produced in the production target pass through the mass slits. Moreover, the second separation stage includes additional strongly focussing beamline elements which contribute further higher-order aberrations. Some direct pions may scatter on beamline apertures, although this process gives a negligible contribution if the apertures are large enough. In addition to the direct pions, kaons decay in the additional length of the second stage, and contribute to a higher π/K ratio.

With the separators turned off there are about 500 times as many pions as kaons; the transmission of the pions through the mass slits with the separators energized should be substantially less than 0.1%. Although protons are as abundant as pions in the raw beam, they undergo much greater deflection by the separators and are effectively removed at the mass slits.

A second source of contamination are muons from pion decay mostly after the first bend, which present a large virtual source to the beam. After one stage of separation the muon intensity is comparable to the kaon intensity since the first mass slit removes the large majority of muons. Since less than 10% of the pions pass through the first mass slit, the major part of the pion beam can no longer contribute to the muon intensity, and muons from pion decay after the first mass slit have an order of magnitude lower intensity; many of them are then removed by the second mass slit.

The decay of neutral kaons and other particles close to the production target produces a large

diffuse source of "cloud" pions. The contribution is difficult to calculate or measure quantitatively, but it is at most a few times the kaon intensity. It is a potential explanation for some part of the observed long tails on pion beam profiles at the mass slits. In a two-stage separated beam, the first mass slit defines a precise source for the second stage and the possible cloud pion contribution is reduced by an order of magnitude.

The addition of a second separation stage works well for the contamination from secondary (π and K decay) processes. The removal of direct pions is complicated by the additional higher order effects in the optics. The major challenge in the design was to address this problem using correcting elements and the inclusion of additional slits.

3. Layout and first-order optics

The LESB3 channel is located in the C proton line of the AGS and views the 6-cm long platinum C1 production target at 0°. Fig. 1 shows the layout and Table 1 lists the beamline elements with their specifications. The length of the channel is 19.6 m, which includes a 2.6-m drift from the last quadrupole to the experimental target.

The optics problems related to the high acceptance and finite target length are illustrated in Fig. 2 which shows the first-order beam envelopes for the central momentum for three points in the production target.

There are three vertical foci, at MS1 and MS2 where the two mass slits are placed, and at F where the experimental target is placed. The vertical magnification is -0.65 at MS1, 0.79 at MS2 and -3.14 at F. There are also three horizontal foci. At HS1 is a momentum-dispersed focus only for the center of the production target; other points in the target are focussed at different positions along the beamline. The momentum slit at HS1 is therefore of limited use in defining the momentum spread but serves mainly to reduce the kaon intensity. At HS2 is a second horizontal focus where all points in the production target are nearly focussed. The beam is only a few cm wide and a slit is placed here. It will be shown in Section 5 that this slit plays a crucial role in removing the pion contamination. The third horizontal focus is at F. The horizontal magnification is -16.45 at HS1, 2.24 at HS2 and -4.38 at F.

The momentum dispersion along the beam reaches a maximum of 5.5 cm-$(\%\Delta P/P)^{-1}$ in Q4 and then gradually declines. It is 5.4 cm-$(\%\Delta P/P)^{-1}$ at HS1. The angular acceptance is 12 msr, and the momentum acceptance is 4.5 $\%\Delta P/P$ FWHM. The beam is achromatic in angle as well as position after the second bending magnet D2.

There is a four-jaw collimator, illustrated in Fig. 3, immediately downstream of the first dipole D1; it is used to reject pions with particular combinations of initial horizontal angle θ and vertical angle ϕ, as will be described in Section 5.1.

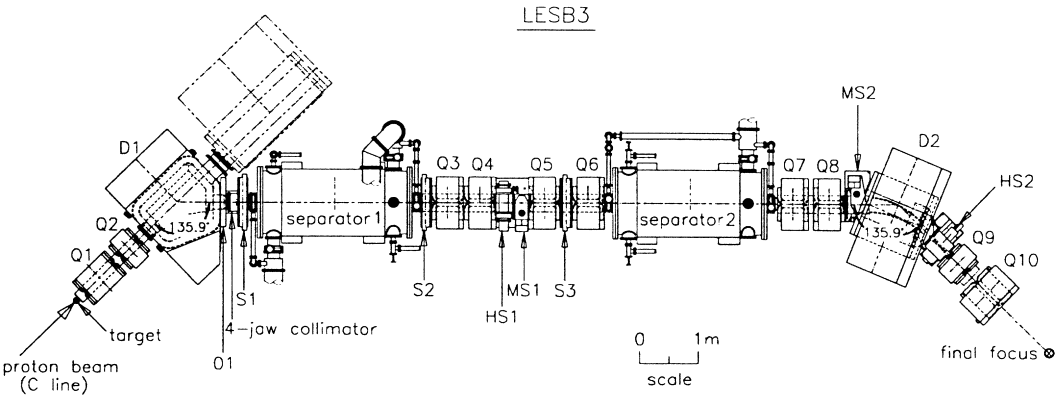

Fig. 1. Layout of LESB3 beamline.

Table 1
Summary of beamline elements. R is the ratio of the turned current to the design value

Element (type)	Length (cm)	Pole radius (cm)	Design pole field (kG)		R
Quadrupole					
Q1(N8Q24)	71.12	10.16	12.757		1.085
Q2(N8Q12)	40.64	10.16	− 9.644		1.068
Q3(12Q12)	41.40	15.24	− 10.661		0.983
Q4(12Q12)	41.40	15.24	8.235		1.000
Q5(12Q12)	41.40	15.24	7.216		1.059
Q6(12Q12)	41.40	15.24	− 10.494		0.965
Q7(12Q12)	41.40	15.24	− 11.680		1.025
Q8(12Q12)	41.40	15.24	14.035		0.995
Q9(N8Q12-3)	40.64	10.16	− 9.150		1.043
Q10(12Q16)	51.56	15.24	12.410		1.040
Sextupole					
S1	16.50	15.24	1.350		1.611
S2	16.50	15.24	− 2.030		0.791
S3	16.50	15.24	− 2.120		0.446
Octupole					
O1	10.0	15.24	2.200		1.082
Dipole	Entr/exit angle to pole face (deg)	Pole gap (cm)	Field (kG)	Bend angle (deg)	R
D1 (sector)	90/90	15.24	18.1	44.1	0.954
D2 (18D36)	22.05/22.05	15.24	19.3	44.1	0.985
Separator	Length (m)	Plate width (cm)	Plate gap (cm)	Plate gap voltage (kV)	Electric field (kV/cm)
SEP1	2.16	40	12.70	575	45.3
SEP2	2.16	40	10.16	550	54.2

4. Higher-order optics

The first-order beam size in the vertical plane is about 2 mm at MS1 and 3 mm at MS2, and realistic mass-slit apertures are 3 mm for MS1 and 4 mm for MS2, for which 70% of the kaons reach the end of the line compared to the situation with the slits open. If only 1% of the pions were to go through, the π/K ratio would be 5, so it is important to minimize the higher-order aberrations as much as possible. The vertical beam size at the mass slits can be expressed in terms of the initial coordinates as

$$y = R_{33}y_0 + R_{34}\phi + A_1\phi\theta + A_2\phi\theta^2 + A_3\phi\theta^3 + B_1\phi\delta + B_2\phi\delta^2 + B_3\phi\delta^3 + \cdots \quad (1)$$

where y_0 is the initial size and R_{33} is the magnification. The first-order matrix element R_{34} is exactly zero at a focus. θ is the initial angle in mr that the projection of a ray on the horizontal plane makes with the beam axis. ϕ is the angle in mr between a ray and its projection on the horizontal plane. δ is the deviation of the momentum from the central momentum $\Delta P/P$ in percent, where P is the central momentum.

The coefficients A_1 and B_1 are large at both mass slits. B_1 can be corrected by a sextupole located where the momentum dispersion is large. This will also affect the value of A_1, which can then be corrected by a sextupole before the first separator where the momentum dispersion is small so that it

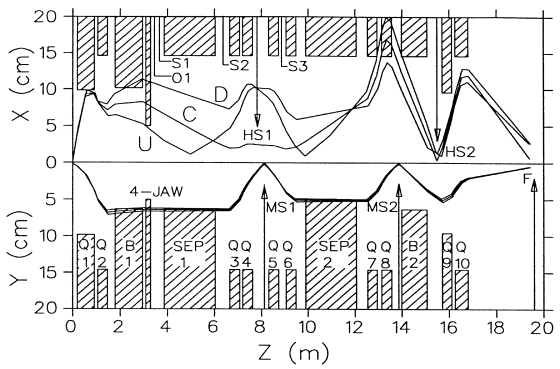

Fig. 2. Calculated first-order horizontal (x) and vertical (y) beam envelopes for the central momentum for three axial positions in the production target. Curve U is for the upstream end, furthest away from the LESB3 beamline, curve C is for the midpoint, and curve D is for the downstream end, closest to the channel.

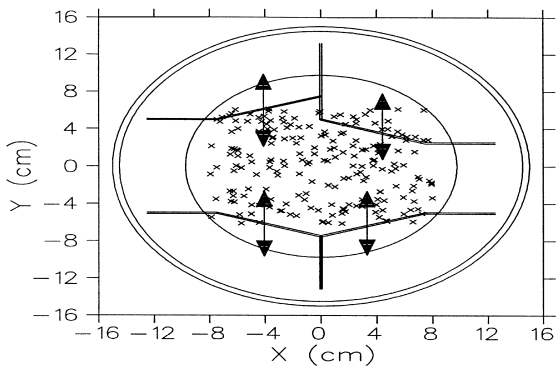

Fig. 3. Sketch of the four-jaw collimator, located immediately downstream of the first dipole D1, showing the independently adjustable vertical jaws, superimposed on the calculated distribution of kaons.

does not affect B_1. In practice, it is possible to correct A_1 only for particles coming from the center of the production target. Sextupole S1 minimizes A_1 at MS1 and this coefficient is then also small at MS2. S2 and S3 minimize B_1 at MS1 and MS2, respectively. The important third-order coefficients are A_2 and B_2 and two octupoles would be necessary to minimize both coefficients at MS1. It was found to be essential only to correct A_2 using one octupole O1 located just after the first bending magnet.

The extent of higher-order corrections necessary was guided by the overall channel performance with respect to kaon flux and pion rejection. Use of a second octupole to correct B_2 gave only a marginal improvement and so was omitted. Further corrections would have been at the level of effects due to terms higher than third order and were not practical. Even the second-order coefficients cannot be corrected fully for the whole length of the production target. The effects of the four-jaw collimator before the first separator and the collimator at the horizontal focus HS2 immediately after the second dipole were sufficient to suppress the remaining pions that go through the mass slits.

Figs. 4 and 5 summarize the effects of the octupole O1 and sextupole S1, respectively. Fig. 4 shows the term $A_2\phi\theta^2$ for $\phi = 20$ mr plotted against θ for the three points in the production target C, U and D. Fig. 4(a) gives the term for the chosen octupole setting of 2.2 kG. Fig. 4(b)–(d) show the effect of varying the octupole between 0.0 and 5.0 kG. The octupole has its largest effect for point D and very little effect for point U. The explanation can be seen in Fig. 2; the horizontal beam size is small at the position of the octupole for U and large for D. Fig. 5 gives similar results for the effects of sextupole S1 on the term $A_1\phi\theta$ for $\phi = 20$ mr.

For each of the three points it gives a band for the values of $A_1\phi\theta$ corresponding to the strength of S1 varying in the range between 0 and 1.35 kG. Clearly, it is not possible to correct the coefficients A_1 and A_2 simultaneously for all points in the production target. Furthermore, rays from different points in the target have varying sensitivity to the strengths of O1 and S1.

Similar studies were performed for the coefficients B_1 and B_2 using S2 and S3 but these coefficients did not show significant sensitivity to the point of origin in the production target.

5. Monte Carlo simulations

5.1. Kaons and pions directly from the production target

The pion contamination in the beam is very dependent on the tails of the pion profiles at the

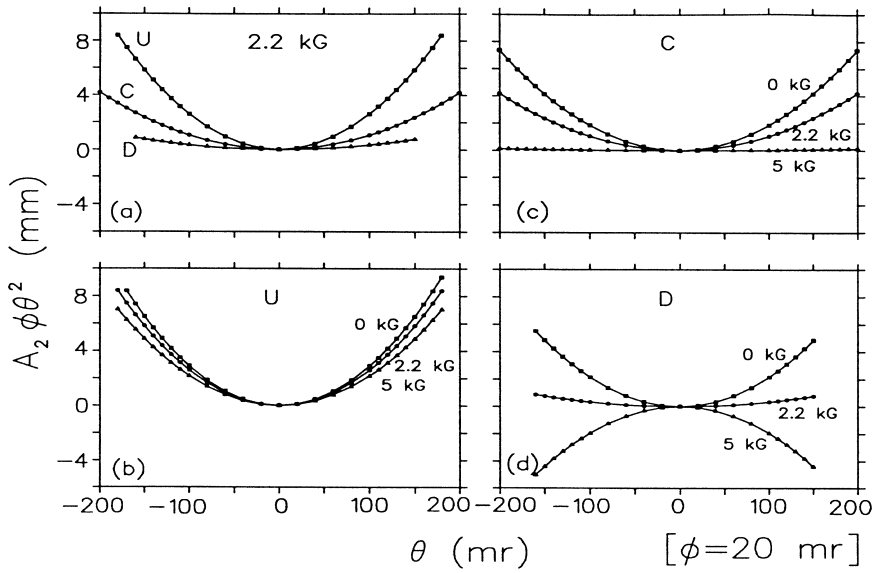

Fig. 4. The effect of the octupole O1 setting on the third-order term $A_2\phi\theta^2$, for fixed $\phi = 20$ mr, as a function of θ: (a) at nominal field strength for three axial positions in the target defined in Fig. 2; (b, c, d), at three field strengths for the three target positions, respectively.

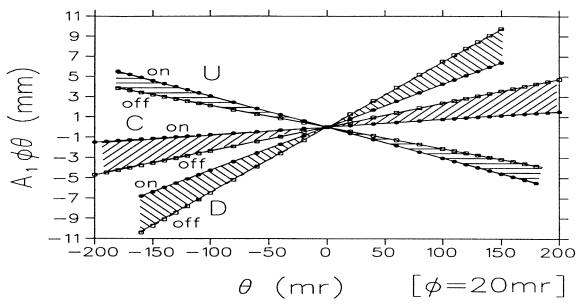

Fig. 5. The effect of sextupole S1 on the second-order term $A_1\phi\theta$ at three axial positions in the target defined in Fig. 2.

mass slits at a level less than 1% of the peak intensity. a reliable simulation requires realistic representations of the field distribution and the fringe fields of magnets, and must take into account the higher order terms of the beam transport. Two programs were used – RAYTRACE [5] and ZGOUBI [4] – which use different methods to trace particles through optical elements. Detailed checks showed that they agreed closely, e.g., at MS2 the vertical position coordinates differed less than 0.1 mm.

The calculations started by randomly choosing the initial coordinates from phase space with ranges for the horizontal angle x' of ± 250 mr, for the horizontal position x, ± 1.5 mm, for the vertical angle y', ± 30 mr, and for the vertical position y, ± 1.2 mm. The momentum bite was $\pm 4\%\Delta P/P$. The length of the production target was 6 cm and all slits were open to begin with. The coordinates of all particles that reached the final focus were saved for six locations along the beam, MS1, MS2, HS1, HS2, the final focus F and at the four-jaw collimator. This was done for 50 000 initial pions and kaons, for which typically 16 000 particles reached the end of the beamline. The program PLOTDATA [6] was used to analyze the results.

Fig. 6(a) shows the vertical beam profile for pions and kaons at MS1. Equal numbers of pions and kaons were run but the kaon curve has been normalized to the experimental ratio of 500 between the pion and kaon intensities when the separators are turned off. The figure also gives profiles for the case with MS2 closed to 4 mm, and for the case with, in addition, the four-jaw collimator partly closed and slit HS2 closed to 2 cm. Fig. 6(b) gives

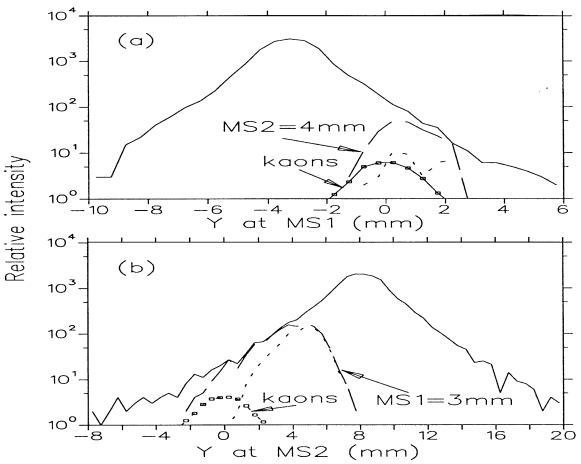

Fig. 6. Calculated vertical beam profiles for pions and kaons at mass slits (a) MS1 and (b) MS2. Solid lines for all slits open, dashed lines for conditions labelled, and dotted lines with in addition, the four-jaw collimator partially closed and HS2 at 2 cm. All slits are open for the kaon peak shown.

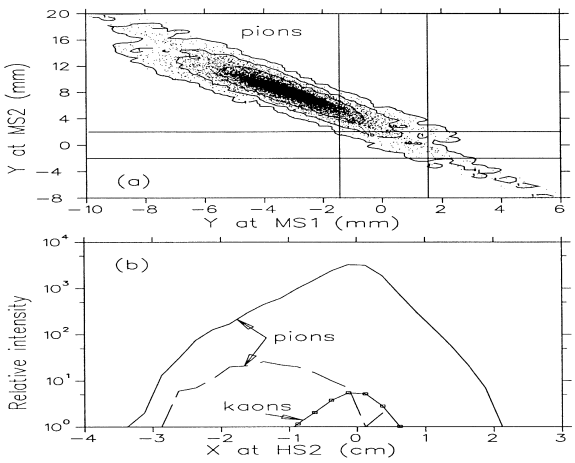

Fig. 7. Calculated distributions of pions in the beamline at the locations of slits. (a) y distributions at MS1 vs. MS2. About 1% of the pions pass through the slit settings indicated. The contours indicate the 1%, 10%, and 50% levels of the pion peak, as a guide to the eye. (b) x distribution at HS2. For pions, the solid line is for slits open, and the dashed line is for MS1 at 3 mm, MS2 at 4 mm. Those same settings are used for the kaons.

similar profiles at MS2. At both MS1 and MS2, pion and kaon peaks are well separated, but the tail of the pion peak overshadows the kaon peak unless the four-jaw collimator and the slit at HS2 are closed.

In Fig. 7(a) we plot y at MS1 versus y at MS2 for pions. About 1% of the pions from the tail of the main distribution remain in the central area corresponding to apertures of 3 mm at MS1 and 4 mm at MS2. Fig. 7(b) shows the horizontal pion profile at HS2 when the mass slits MS1 and MS2 are open and closed to 3 and 4 mm, respectively. In the latter case the pions which reach HS2 are mainly distributed on one side of the beam axis.

Fig. 8(a) and (b) give some indication of the reason that those pions pass through the mass slits. Fig. 8(a) plots y at MS2 versus the axial point of origin in the production target. The pions which go through the 4-mm aperture of MS2 come mainly from the upstream part of the production target. Fig. 8(b) plots y at MS2 versus θ. The points are for all pions and the boxes are for pions coming from the central 1 cm of the target. Again, it is clear that the main reason for the contamination is the length of the target.

Fig. 9(a) and (b) give x vs. y at the four-jaw collimator with the mass slits closed to nominal

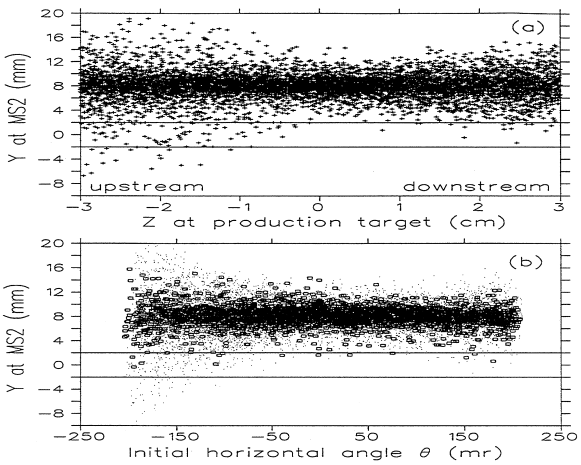

Fig. 8. (a) Calculated y at MS2 for pions vs. axial position of origin in the production target, (b) y at MS2 vs. θ for all pions (dots) and those only from the center 1 cm in the target (boxes).

values. The points are for kaons and the boxes for pions, showing the pions mainly in the upper right corner and a few in the upper left corner. Fig. 3 shows a schematic drawing of the four-jaw collimator indicating the independent movement of

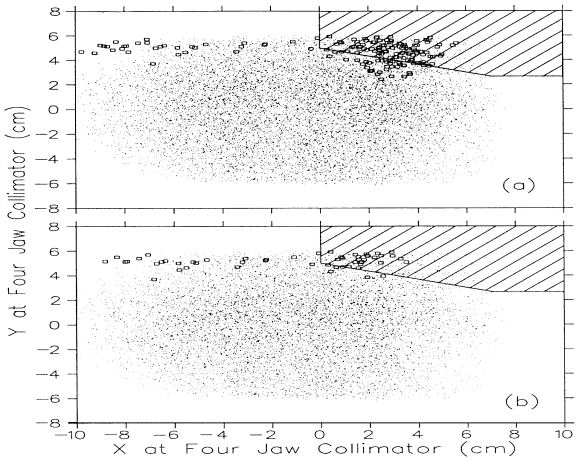

Fig. 9. Scatterplots of calculated x vs. y for kaons (dots) and pions (boxes) at the position of the four-jaw collimator, with the slit HS2 (a) open, and (b) at 2 cm. The crosshatched area shows the nominal position of the upper right jaw of the four-jaw collimator. MS1 and MS2 are at 3 and 4 mm, respectively.

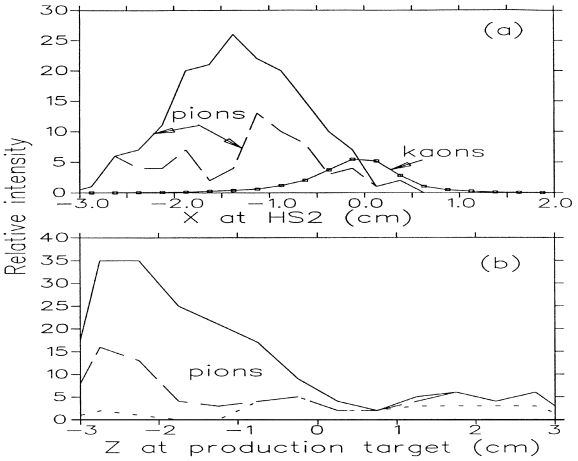

Fig. 10. Calculated (a) x for pions and kaons at HS2, and (b) pion intensity as a function of axial position of origin in the target. Solid and dashed lines in (a) and (b) are for the four-jaw collimator open and set as shown in Fig. 9, respectively. The dotted line in (b) shows the additional effect of closing HS2 to 2 cm.

the four jaws. The crosshatched area in Fig. 9 indicates the position of the upper right jaw set to cut out a large fraction of the pions. Fig. 9(b) is similar to Fig. 9(a) except that HS2 is closed to 2 cm.

Fig. 10(a) gives the horizontal pion spot at HS2 with the mass slits closed showing that this distribution dominates the kaon distribution. When the four jaw collimator is closed as indicated by the crosshatched area in Fig. 9, the pion distribution is much smaller. The slit at HS2 can cut out a substantial part of these pions while reducing the kaon intensity only marginally. Fig. 10(b) shows the pion intensity as function of the point of origin in the production target. It can be seen that the combined effect of the 4-jaw collimator and the slit at HS2 effectively cut the pion contamination originating in the upstream region of the target.

5.2. Cloud pions

The effect of two-stage separation on the transmission of cloud pions from K^0 decay was investigated by assuming a source of $4\times4\,cm^2$ at the production target. The vertical beam profile at MS2 is shown in Fig. 11 for MS1 open and closed to 3 mm. The transmission through an aperture of

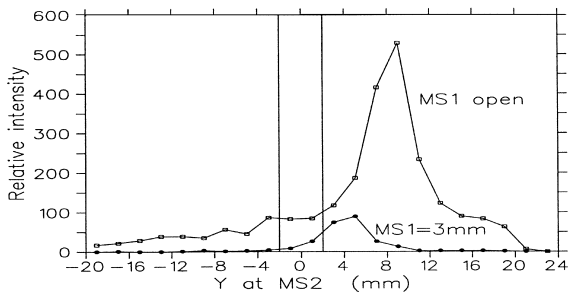

Fig. 11. Calculated y distribution at MS2 of cloud pions from K^0 decay near the production target for two settings of MS1. The nominal setting of MS2 is shown by the vertical lines.

4 mm at MS2 is reduced by a factor 5.3 if MS1 is closed to 3 mm. Fig. 12 shows results of a calculation of the horizontal beam profile at HS2 for cloud pions. MS1 was 2.4 mm wide, MS2 was 2.8 mm wide, and the four-jaw collimator was open. Closing the upper right jaw of the four-jaw collimator gives the line marked by the boxes, which partly coincides with the line for the open case. A 2-cm wide slit at HS2 will remove most of the remaining cloud pions, although as will be further discussed in Section 6, in practice this is a small effect.

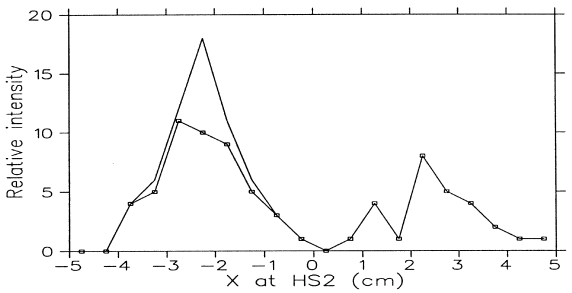

Fig. 12. Calculated x distribution of cloud pions at HS2 with the four jaw collimator open and with the upper-right jaw closed (boxes). MS1 and MS2 are at 2.4 and 2.8 mm, respectively.

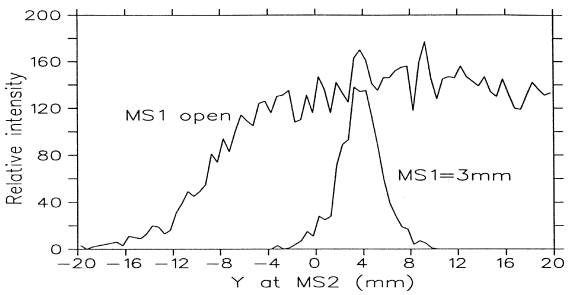

Fig. 13. Calculated y distribution at MS2 of muons from pion decay.

5.3. Muons from pion decay

The contribution to the contamination of muons from pion decay was calculated. If MS2 is closed to 4 mm, the μ/K ratio is 1.1. When MS1 is closed to 3 mm the ratio is reduced to 0.23. Fig. 13 shows the vertical muon profile at MS2 for MS1 open and closed to 3 mm.

6. Comparison with measurements

Measurements of the vertical beam profile for the kaon peak and for the tail of the pion distribution were made at the two mass slits by scanning the beam through narrow 1.0-mm wide mass slits using the magnetic fields of the separators. At HS2 the horizontal beam profile was determined from the total rate as a function of slit position for each of the left and right slits. Several settings for the four-jaw collimator were used – open, closed and with only the upper right jaw closed.

In order to normalize the measured beam profiles for comparison with calculations, the relative pion and kaon rates were measured. Since this was done at high proton intensity it was necessary to reduce the counting rate for the pion measurements by closing the four-jaw collimator, and the slits at HS1 and HS2. MS1 was open and MS2 was 6 mm wide. Even so, with the high counting rate when the pions were steered through MS2, a deadtime of 22% had to be taken into account. The result was that the pion rate was 526 times the kaon rate.

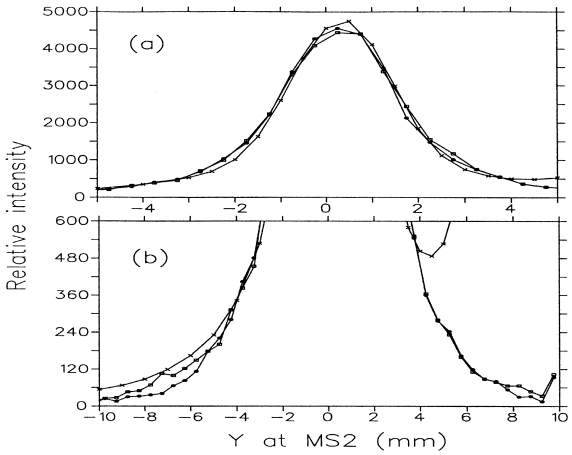

Fig. 14. Measured y profile for kaons (crosses) at MS2 with MS1, HS2, and the four-jaw collimator open, compared with calculated distributions for two settings of the multipoles, before (boxes) and after (dots) optimizing to the values shown in Table 1. (b) is an expanded view of (a) to show the tail regions.

Fig. 14(a) shows the kaon profile at MS2 with MS1, the four-jaw collimator and HS2 open. The calculated peaks were obtained using an initial vertical spot at the target of 2.4 mm and were normalized to the measured peak using the total rate in the area of $\pm$ 3 mm around the peak. The crosses give the measured peak after optimization; the two other curves show the calculated distribution with initial design settings of the multipoles and with the very different final values obtained after optimization, respectively. The tails are shown in more detail in Fig. 14(b). Beyond about $+$ 4 mm the measured tail is swamped by misidentified

pions from the main pion peak at + 7.5 mm. On the negative side for smaller than about − 5 mm misidentified pions from the tail of the pion distribution begin to dominate the kaon rate. At the level of a few percent of the peak intensity the peak shape measured in the beamline is in very good agreement with the design expectations.

Fig. 15(a) and (b) show the measured (boxes) and calculated vertical beam profiles at MS2 for the pions and kaons for the four-jaw collimator open and all four jaws fully closed, respectively. The calculated pion distribution includes the muons from pion decay. The calculated muon distribution is given separately by the black dots. For the open case the direct pions plus the muons represent the tail of the pion distribution fairly well. Beyond − 4 mm the calculated tail consists almost entirely of muons but it underestimates the observed tail. In the closed case, the calculated tail is entirely due to muons, since direct pions make a negligible contribution. Again the observed pion distribution is about double the prediction.

Although muons and direct pions can explain a significant part of the observed pion distribution, there is evidently a contribution which could be from an other source. One possibility is pions which are created by the decay of kaons and other particles near the production target. Such a distribution would be expected to have a long tail, which would be consistent with the missing contribution in the open case. Moreover, the distribution may be peaked near the vertical center of the production target and this could also explain the difference between calculation and measurement at the position of the kaon peak in the closed case. This contribution attributed to cloud pions is at most comparable to the kaon rate with MS1 open. With MS1 closed the cloud pion rate should be a factor of 5 smaller.

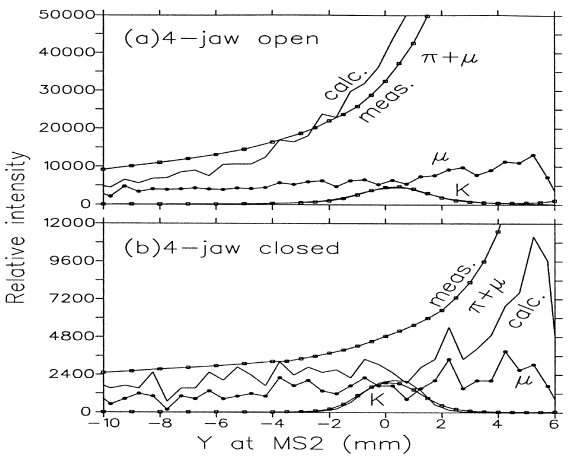

Fig. 15. Measured (boxes) and calculated (as labelled) y distributions at MS2 for the four-jaw collimator (a) open and (b) fully closed.

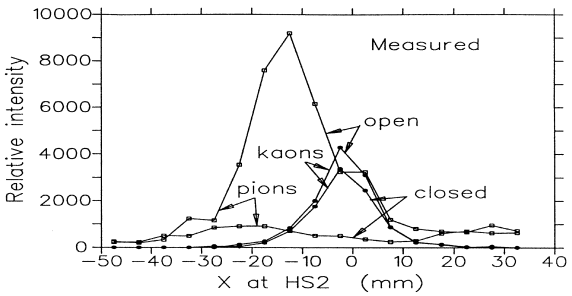

Fig. 16. Measured kaon and pion distributions at HS2 with the four-jaw collimator open and upper-right jaw closed. Compare with Fig. 10(a).

Fig. 16 gives the measured pion and kaon distributions at HS2 for MS1 and MS2 set at 2.4 and 3.0 mm, respectively, and for the four-jaw collimator open and upper right jaw closed. These distributions are in good agreement with the design predictions shown in Fig. 10(a).

7. Conclusions

A high-flux, high-purity 800-MeV/c kaon beam was designed using detailed analysis of higher-order optics to determine a combination of magnetic element corrections and additional apertures to control the effects of aberrations. The design technique reliably predicted the overall performance of the beamline as built.

Acknowledgements

We are grateful to the engineering and technical staff of BNL for their commitment to speedy

construction of the beamline. We acknowledge the contributions of engineers G. Clark and A. Otter of TRIUMF to the design and construction of the front end beamline elements. We also thank other members of the E787 collaboration who assisted in the beamline commissioning. This work is supported by funding from the US Department of Energy, and from the Canadian National Research Council and Natural Sciences and Engineering Research Council.

References

[1] C.F. Germain, D.F. Leroy, D.J. Simon, CERN Report CERN/MPS-MU-SD 70–4.
[2] S. Adler et al., Phys. Rev. Lett. 76 (1996) 1421.
[3] P.H. Pile et al., Nucl. Instr. Meth. A 321 (1992) 48.
[4] F. Meot, ZGOUBI, CERN Report SL/94-82 (AP) and Saturne Note LNS/GT/93-12.
[5] S. Kowalski, H.A. Enge, RAYTRACE, Massachusetts Institute of Technology, Cambridge MA 02139, USA, July 1987.
[6] J.L. Chuma, PLOTDATA, TRIUMF Design Note TRI-CO-87-03a.